Atomic-layered MoS_{2} on SiO_{2} under high pressure: Bimodal adhesion and biaxial strain effects

R. S. Alencar, K. D. A. Saboia, D. Machon, G. Montagnac, V. Meunier, O. P. Ferreira, A. San-Miguel, and A. G. Souza Filho

Phys. Rev. Materials **1**, 024002 — Published 12 July 2017

DOI: 10.1103/PhysRevMaterials.1.024002

Atomic layered MoS_2 on SiO_2 under high pressure: bimodal adhesion and biaxial strain effects

R. S. Alencar,[1,2] K. D. A. Saboia,[2,3] D. Machon,[2] G. Montagnac,[4] V. Meunier,[5] O. P. Ferreira,[1] A. San-Miguel,[2] and A. G. Souza Filho[1]

[1]*Departamento de Física, Universidade Federal do Ceará, Fortaleza, Ceará, 60455-900 Brazil*

[2]*Université de Lyon, F-69000 Lyon, France and Institut Lumière Matière, CNRS, UMR 5306, Université Lyon 1, F-69622 Villeurbanne, France*

[3]*Laboratório de Telecomunicações e Ciência e Engenharia de Materiais LOCEM, Departamento de Física, Universidade Federal do Ceará, Fortaleza, Sobral, Ceará, Brazil*

[4]*Laboratoire de Géologie de Lyon, Ens de Lyon, CNRS UMR5276, 46 allé dItalie, BP 7000, 69342 Lyon Cedex 07, France*

[5]*Department of Physics, Applied Physics, and Astronomy, Rensselaer Polytechnic Institute, Troy, NY 12180, USA*

(Dated: June 9, 2017)

Abstract

The stacking effect on the E^1_{2g} and A_{1g} vibrational modes of mechanically exfoliated MoS_2 samples supported on SiO_2 were investigated by non-resonant Raman spectroscopy at high pressure conditions. Splitted E^1_{2g} and A_{1g} modes were observed for single and bilayered samples whereas such splitting disappears for higher number of layers. The differences on the E^1_{2g} pressure coefficients allowed to interpret the observed splitting as due to the presence of two types of regions corresponding to a high and a low conformation of MoS_2 to the substrate roughness. The difference in the pressure coefficient appears then as due to the biaxial stress introduced via the substrate compression. Such effects were not observed for the A_{1g} mode due to the its vibration symmetry. This out-of-plane vibration is mainly affected by the normal stress that corresponds to pressure transmitted by the pressure transmitting medium.

INTRODUCTION

The discovery of graphene [1] opened a new and increasing research area on two-dimensional (2D) materials both related to fundamental issues and to the many potential applications [2, 3]. Among layered materials (LMs) [4–10], the transition metal dichalcogenide (TMD) MoS_2 have attracted attention due to its remarkable physical properties, as high mobility ($\mu > 200$ cm^2 V^{-1} s^{-1}) [11] and Young's modulus (0.33 TPa) [12]. Besides, differently from graphene, MoS_2 presents an intrinsic direct band gap of 1.8 eV [13], on the limit of monolayer-thickness, which makes it a good candidate to complement (or even substitute) graphene in electronic [11, 14] and optoelectronic [15–17] applications.

Bulk MoS_2 single crystal is a semiconductor with a 1.3 eV indirect band gap [18]. It is built up from the stacking of S-Mo-S (monolayer) layers by weak van der Waals forces in a Bernal arrangement [19]. Each monolayer is formed by two hexagonal planes of sulfur (S) atoms sandwiching a hexagonal plane of molybdenum (Mo) atoms linked via ionic-covalent bonds arranged in a trigonal prismatic structure [18, 20]. In the bulk form it belongs to space group *P3m1* (point group D_{6h}), whereas in the monolayer limit it belongs to *P6m2* (point group D_{3h}), and as a consequence monolayer MoS_2 does not present an inversion symmetry [21]. This lack of inversion of symmetry splits the valence bands due to the spin-orbit interaction, opening possibilities for MoS_2 as a suitable material for valleytronics [22]. The electronic gap of MoS_2 can in fact be tuned by the number of layers [18].

The young and rapidly growing field of 2D-dimensional systems science relies very often on the study of 2D-system supported on a substrate. It becomes then fundamental to understand how the interaction with the substrate modifies the intrinsic properties of the system and its response to various solicitations. Pressure application allows to continuously increase the interaction between the 2D-system and its environment, constituting then a method of choice to understand such effects [23]. In this work the evolution of phonon modes with pressure will evidence that such interaction can be extremely inhomogeneous and even having a bimodal character.

Raman spectroscopy is a nondestructive tool widely used to identify the numbers of layers of MoS_2 thanks to its sensitivity to the MoS_2 thickness variation [24, 25]. Bulk MoS_2 presents four first-order Raman active vibrational modes in the center of the Brillouin zone, E^2_{2g}, E_{1g}, E^1_{2g} and A_{1g}, located at about 32 cm^{-1}, 286 cm^{-1}, 383 cm^{-1} and 408 cm^{-1},

respectively [20, 26]. With the exception of the E^2_{2g}, all modes correspond to intralayer vibrations in a S-Mo-S layer, whilst the interlayer mode E^2_{2g} comes from the respective atomic movement of two adjacent S-Mo-S layers to each other. The E_{1g} mode is forbidden in a back-scattering geometry perpendicular to the basal plane. The E^1_{2g} mode results from the in-plane vibration of the sulphur and molybdenum atoms in opposite directions, whereas the A_{1g} mode is related to out-of-plane vibrations of the sulphur atoms [20, 25, 26]. Because of experimental limitations, we investigated here only the behaviour of E^1_{2g} and A_{1g} modes in n-layered MoS_2.

The use of pressure has been an effective method to probe structural [7, 27–30], electrical [27, 31–33] and optical [13, 34–36] properties of MoS_2. It is known that the single crystal (as well as powder) of MoS_2 experiments an electronic and structural phase transition (2Hc to 2Ha) under high pressure ($\sim$ 20 GPa) governed by the sliding of adjacent S-Mo-S layers, leading to a semiconductor-metal transition when the phase change is completed [27, 33]. For bilayer MoS_2, high pressure photoluminescence measurements were used to clarify the optical transitions that were not well established [13]. In a recent report, high pressure Raman measurements were used to investigate monolayer MoS_2. There, it was observed a pressure-induced phase transition characterized by the appearance of two new peaks located at 200 cm^{-1} and 240 cm^{-1} at 5.8 GPa. The new phase was suggested to be similar to the 1T'-MoS_2 one, in which the sliding of S atoms inside the S-Mo-S layer is caused by a distortion of the unit cell [29].

Despite the availability of many studies about the influence of the stacking on the physical properties of MoS_2, the influence of stacking on the high pressure response of MoS_2 remains less explored and constitutes an original method to study the interactions of LMs with their environment [37]. In this study we present the influence of the interlayer interactions due to thickness variation on the vibrational modes of the mono-, bi-, tri- and many layers of MoS_2 submitted to hydrostatic high pressure by means of non-resonant Raman spectroscopy.

METHODOLOGY

Experimental setup and sample characterization

Few layers of MoS_2 were obtained by standard mechanical exfoliation [38] from single crystal (SPI Supplies) and deposited on thin (50 μm of thickness) cleaned silicon substrate with 300 nm of silicon oxide. The identification of the number of layers was done by optical contrast and Raman spectroscopy, Figure 1. Raman spectra was acquired using the LabRAM (during the pressure cycle) and Renishaw (ambient conditions) systems with energy excitation of 2.33 eV (532 nm) and power setted at $\sim$ 0.5 mW on the entrance of the high pressure device to avoid thermal effects [39]. The laser was focused with a 50x magnification objective lens and the signal was dispersed by a grating of 1800 grooves/mm.

The Raman frequencies of in-plane E^1_{2g} (open red squares) and out-of-plane A_{1g} vibrational modes (open red circles) as a function of the number of layers is shown in Figure 1. Also, their differences A_{1g} - E^1_{2g} (open blue triangles) and the results from Ref. [24] (filled red and blue symbols) were placed for comparison. Our results show an excellent agreement with those found by Lee [24]. The Raman spectra was taken from the regions limited by red dashed lines on the inset of Figure 1, which are labeled with their respective number of layers. Here the fits were done with a single component to allow for comparison with the data of Ref. [24] in spite that as will be discussed later two components are present for each peak.

High pressure experiments were performed using a diamond anvil cell pressure device with diamond anvils having a culet size of 700 μm. The MoS_2 sample consisting on regions with 1, 2, 3 and many layers deposited by mechanical exfoliation on a thin SiO_2/Si substrate was loaded in a cylindrical pressure chamber with diameter of $\sim$ 315 μm and thickness of $\sim$ 100 μm in a pre-indented stainless steel gasket placed between the two diamond anvils. A 4:1 methanol-ethanol mixture, that is known to remain liquid and hydrostatic up to 10.5 GPa [40], was used as pressure transmitting medium (PTM). A small ruby chip was placed together with the sample and PTM inside the pressure chamber to calibrate the pressure by standard ruby luminescence R1 line [41].

Spectra were collected for each region of the sample in the same hydrostatic conditions up to a maximum pressure of 8.7 GPa.

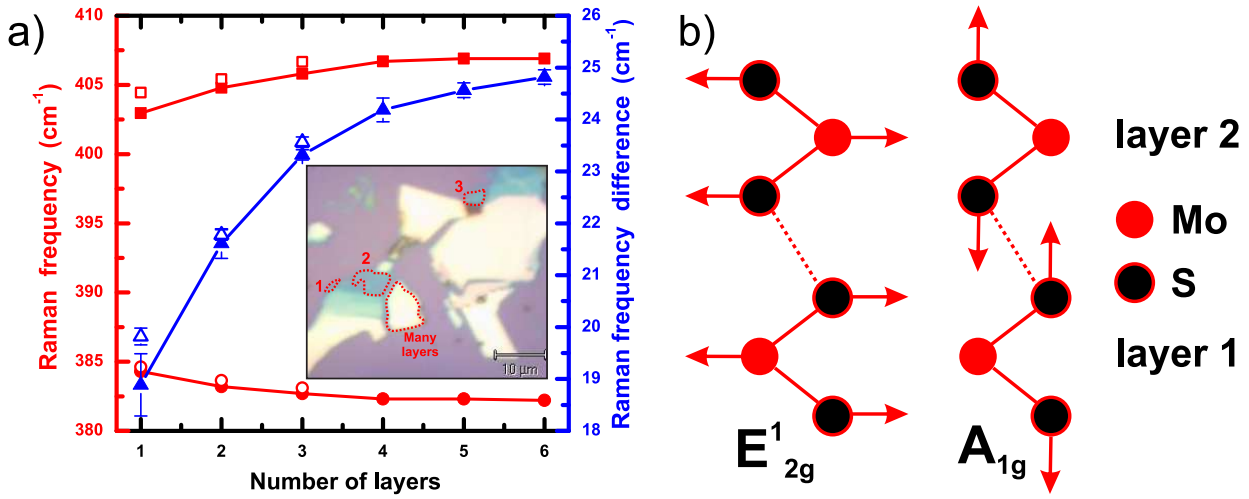

FIG. 1. Identification of the MoS_2 thickness by comparing the frequencies of in-plane E^1_{2g} (red squares) and out-of-plane A_{1g} (red circles) vibrational modes of our sample (open symbols) with the results from Ref.[24], as well as their frequency differences A_{1g} - E^1_{2g}. The areas limited by the red dashed lines show the regions in which the Raman spectra were taken and the numbers correspond their number of layers. (b) Sketch of the atomic displacements of E^1_{2g} and A_{1g} modes.

RESULTS

Figure 2 shows the Raman spectra of monolayer (a), bilayer (b), trilayer (c) and many layers (d) of MoS_2 ranging from ambient conditions (AC) up to 8 GPa. We see that for the monolayer and the bilayer samples, from ambient conditions, the vibrational modes E^1_{2g} and A_{1g} (and their corresponding ones for odd number of layers, E' and A_1, respectively) need to be fitted with two Lorentzian functions each one. We have labelled these components as ${E^1_{2g}}^{(h)}$ (E'$^{(h)}$), ${E^1_{2g}}^{(\ell)}$ (E'$^{(\ell)}$), ${A_{1g}}^{(h)}$ (${A_1}^{(h)}$) and ${A_{1g}}^{(\ell)}$ (${A_1}^{(\ell)}$). The suffix can be for the moment considered as arbitrary, but correspond to "in high conformation"(h) and "in low conformation" (ℓ) as will be explained later. With increasing pressure, the intensity ratio between the "(h)" and the "(ℓ)" components evolve. In particular in the case of the monolayer sample the intensity of the "(h)" component becomes very weak after 0.7 GPa with the E'$^{(h)}$ peak becoming undetectable beyond 1.6 GPa. The effect is less marked for the bilayer sample where the two components are always present at all the measured pressures.

For the trilayer and the sample having many layers (which can be assimilated to bulk MoS_2) we do not observe such splitting. The peaks in Figure 2c and d are labelled ${E^1_{2g}}^{(\ell)}$ (E'$^{(\ell)}$), ${A_{1g}}^{(\ell)}$ (${A_1}^{(\ell)}$). We note in Figure 2b and c that for the bilayer and trilayer sample, a new peak, which is labeled "B" is visible from ∼5 GPa with its intensity increasing with

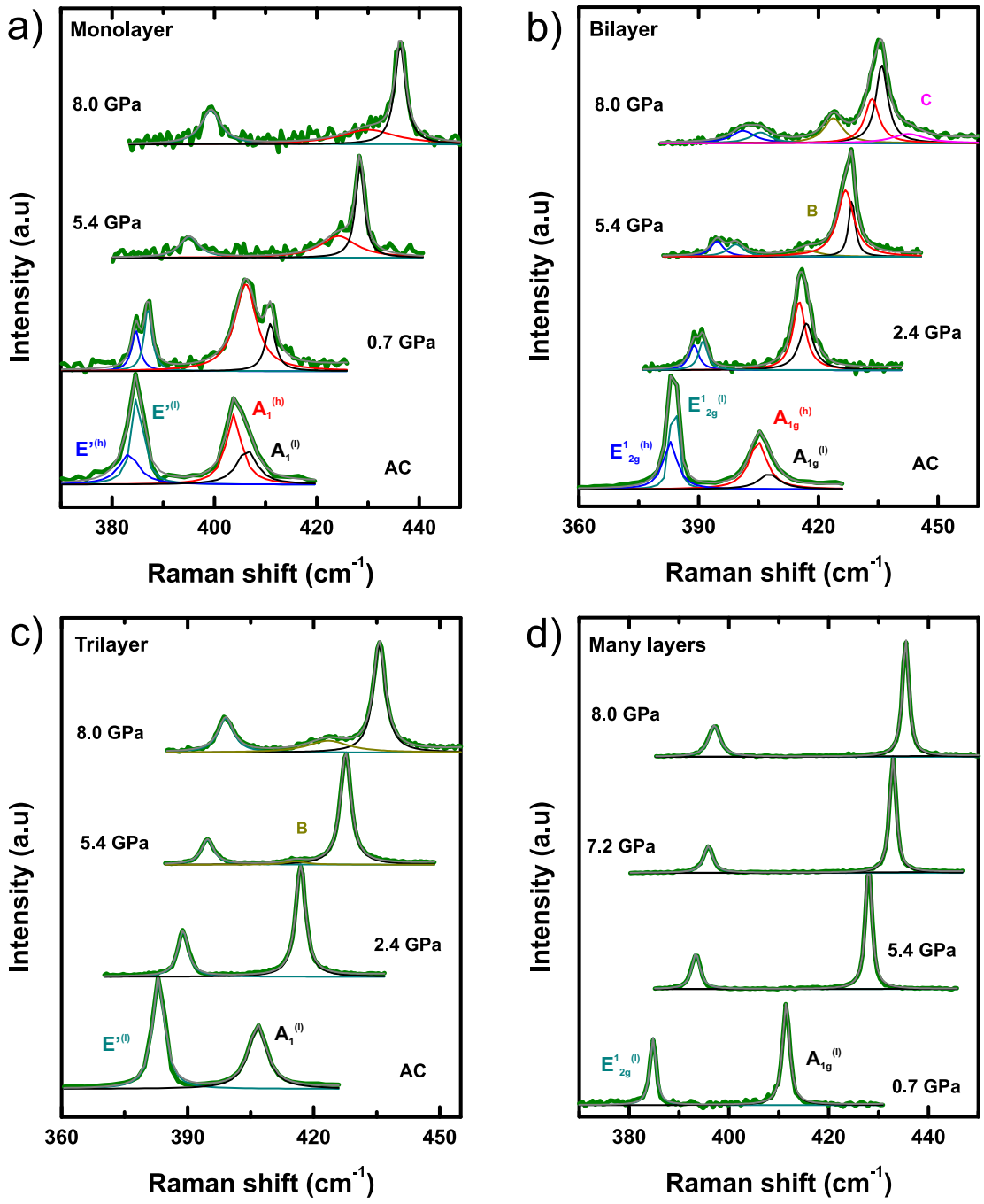

FIG. 2. MoS_2 Raman spectra collected at different pressure points for monolayer (a), bilayer (b), trilayer (c) and many layers (d). When two components of the in-plane E^1_{2g} (E') and out-of-plane A_{1g} (A_1) modes are found we use the suffix "(h)" and the "(ℓ)".

pressure. Finally in the bilayer sample it is also observed a broad and weak intensity peak in the higher energy side of the A_{1g} band appearing from 7.2 GPa. We label that peak C (Figure 2b).

To study the pressure dependence of the vibrational modes, we fit each mode with a

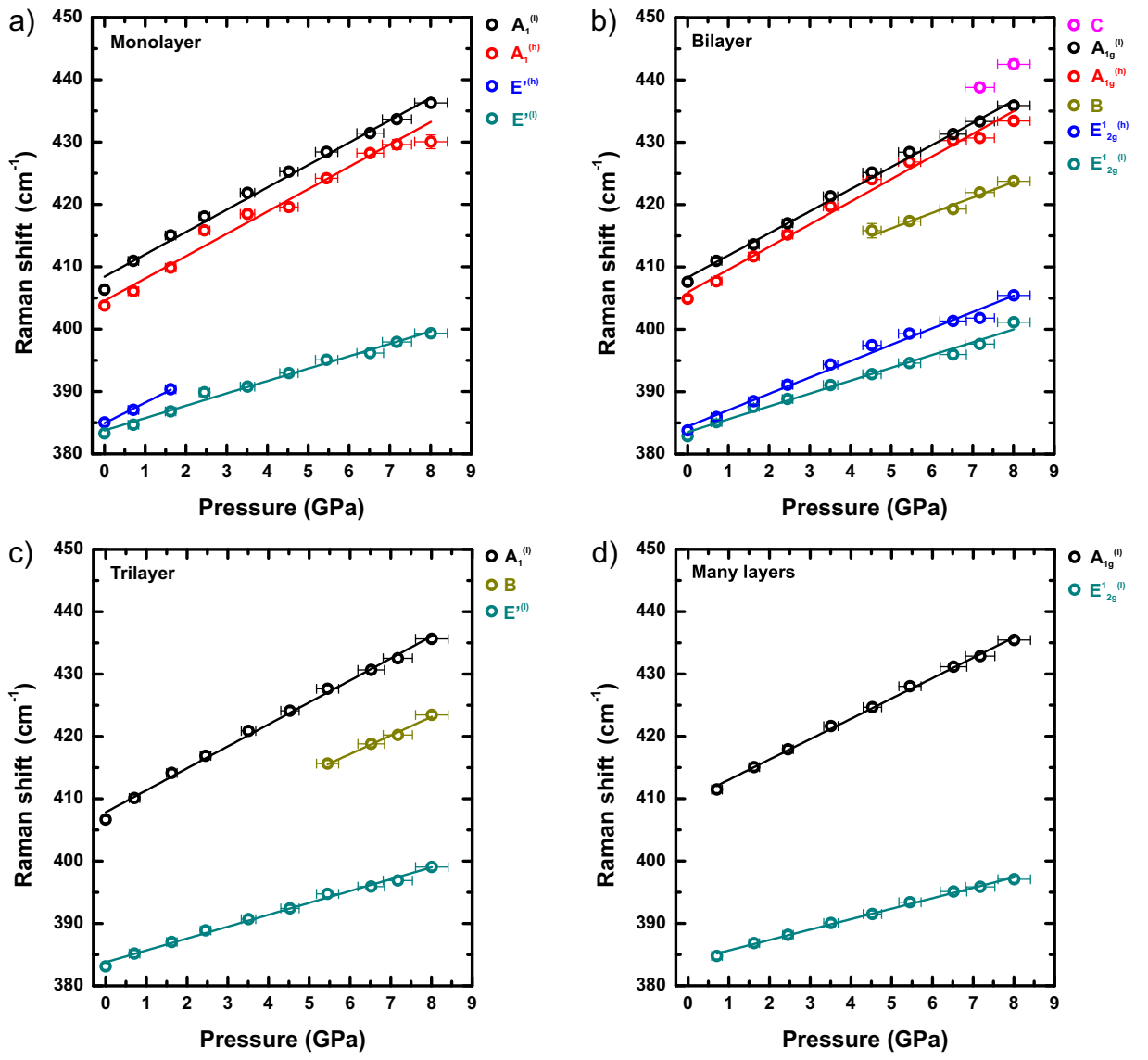

FIG. 3. Pressure dependence of MoS_2 Raman frequencies for all observed Raman vibrational modes and the corresponding linear fits (except for the C mode in the bilayer which did not present a number of points enough to make a fitting reliable) for monolayer (a), bilayer (b), trilayer (c) and many layers (d) samples

Lorentzian function (Figure 2) for all pressure points acquired and plot their Raman frequencies as a function of pressure as shown in Figure 3. Here, all vibrational modes present linear and positive pressure coefficients, which are given in Table I together with the value of their frequencies at ambient pressure.

The obtained linear coefficient of the E^1_{2g} mode of 1.7±0.1 cm^{-1}/GPa^{-1} for the many-layer sample is in rather good agreement with the values found in the literature for bulk MoS_2 which vary between 1.8 to 1.9 cm^{-1}/GPa^{-1} [34, 42, 43]. The corresponding A_{1g} value

TABLE I. Assignment of MoS_2 vibrational modes and their frequencies intercept (ω_0), as well as their pressure coefficients ($\partial\omega/\partial P$). The Raman modes labeled B could not be unambiguously assigned.

n	$E^1_{2g}{}^{(\ell)}$ ($E'^{(\ell)}$)	$E^1_{2g}{}^{(h)}$ ($E'^{(h)}$)	$A_{1g}{}^{(\ell)}$ ($A_1{}^{(\ell)}$)	$A_{1g}{}^{(h)}$ ($A_1{}^{(h)}$)	B
			ω_0 (cm^{-1})		
1	383.8	384.9	408.4	404.5	-
2	383.5	384.4	408.3	405.9	403.8
3	383.8	-	407.8	-	399.2
many	384.0	-	409.8	-	-
			$\partial\omega/\partial P$ (cm^{-1} / GPa)		
1	2.0±0.1	3.3±0.4	3.6±0.1	3.6±0.1	-
2	2.1±0.1	2.6±0.1	3.5±0.1	3.6±0.1	2.5±0.2
3	1.9±0.1	-	3.5±0.1	-	3.0±0.3
many	1.7±0.1	-	3.3±0.1	-	-

of the many layer sample, 3.3±0.1 cm^{-1}/GPa^{-1}, is on its side slightly smaller than the bulk values found in the literature which range from 3.6 to 4.0 cm^{-1}/GPa^{-1} [34, 42, 43].

The obtained frequency of the B mode and its pressure coefficient are close to the values observed in bulk MoS_2 for the B_{1u} mode (ω_0= 402.9 cm^{-1} and $\partial\omega/\partial P$= 2.2 cm^{-1}/GPa^{-1} [34]. This mode is not Raman active and in fact it is not observed in all bulk experiments. The activation of this mode in the bilayer and trilayer sample at pressures of about 5 GPa remains to be understood. The C mode, only observed in the last two spectra of the bilayer sample lies at $\sim$ 10 cm^{-1} above the A_{1g} mode. This is also the case of dispersive modes observed in bulk MoS_2 interpreted involving multiple phonon scattering with polariton coupling [34]. In the following our discussion will be centered on the E^1_{2g} and A_{1g} modes.

DISCUSSION

Previous studies in mono- and bilayer MoS_2 deposited on flexible substrates submitted to uniaxial strain showed a splitting of the E^1_{2g} modes which was interpreted as a breaking of the degeneracy in the initially degenerated in-plane mode E^1_{2g} [44, 45]. Such breaking of the degeneracy was interpreted as due to van der Waals interactions at the substrate-sample interface. For bulk MoS_2 the in-plane modes E^2_{2g} and E^1_{2g} also exhibit splitting at about 20 GPa caused by the modification in the interlayer stacking through the sliding between adjacent S-Mo-S layers [27, 33, 34]. Similar splits for both vibrational modes E^1_{2g} and A_{1g} in

monolayer MoS_2 under high pressure have been observed [29]. There, they were explained by the deformation of the S-Mo-S structure caused by different interactions of the silicon substrate and PTM with the S layers, which can induce sliding of Mo or S layers within the monolayer, leading to different Mo-S bond lengths and consequently to different vibration energies. Our measurements on monolayer MoS_2 and those of Ref. [29] are in excellent agreement. Nevertheless our observation of the presence of the same type of splitting of the E^1_{2g} and A_{1g} modes also for the bilayer sample and its absence for a higher number of layers lead us to a different interpretation.

In the case of graphene, Nicolle *et al.* [37] observed a different response in the high pressure Raman signal for mono- and bilayer in comparison with trilayer samples. Monolayer and bilayer graphene undergo a biaxial strain resulting from the substrate volume reduction on pressure application. The graphene ability to conform to the SiO_2 substrate roughness is the key point for such biaxial transmission. Unlike the mono- and bilayer samples, trilayer graphene undergoes a 3D hydrostatic compression by the PTM due to the unbinding state between SiO_2 substrate-trilayer graphene, related to the higher bending modulus of the 3-layered sample.

The parameters governing the conformation of a 2D-system to a rough substrate are the adhesion energy (γ_n), the bending modulus of the 2D n-layer system (D_n) and the characteristic curvature radius of the surface (k_s). It has been shown [46] that in 2D-membranes a single dimensionless parameter, $\alpha = (k_{eq}/k_s)^{1/2}$ which compares the typical curvature of the substrate with the adhesion equilibrium curvatures, $k_{eq} = (2\gamma_n/D_n)^{1/2}$ governs the conformation of the 2D-membrane to the surface. Perfect adhesion is expected for $\alpha > 0.8 - 0.86$ [46] which in fact for graphene on SiO_2/Si, with a characteristic $k_s = 0.3$ nm^{-1} leads to an unbinding when the number of graphene layers is increased from 2 to 3 [37]. The substrates used in the present work are in fact the same used in Ref. [37]. In the case of single-layer MoS_2 its bending modulus, D_1, has been calculated to be 9.61 eV, i.e., ~ 7 times higher than the value for single-layered graphene [47]. On the other side, it has been shown in AFM experiments [48] that the adhesion energy of MoS_2 on SiO_2 is smaller than for graphene on SiO_2. The report between graphene and MoS_2 D_1 values being more important than the report between D_1 and D_2 in graphene (see later), we may expect that an unbinding transition of MoS_2 on SiO_2 can already take place in the monolayer system. This is supported by AFM observations [49] in which the roughness ratio between

single-layer MoS_2 on SiO_2 and bare SiO_2 was found to be 0.56 while the equivalent ratio reported for graphene is 0.9 or higher [50]. We then expect that for $n = 1$ MoS_2 can already be found in a low conformation state. The membrane model here referred [46] is based on the description of the surface roughness as a periodic fixed curvature structure. Real roughness leads to a statistical distribution of curvature values and we admit that MoS_2 can be found in alternating regions in high conformation with the SiO_2 substrate (h) and in low conformation with the substrate (ℓ). The two components of both the E^1_{2g} and A_{1g} modes in our sample can be explained by considering this particular situation. In the h-region the MoS_2 layer, in adhesion with the substrate, undergoes a biaxial strain due to the volume reduction of the substrate on pressure application. On the other hand, in the ℓ regions the PTM flows through unbinded regions and then the MoS_2 layer experiments a reduced biaxial strain, with a response closer to hydrostatic.

In that way the two components appearing in the E^1_{2g} and A_{1g} in mono and bi-layer MoS_2 can be well interpreted as due to the presence of both high and low conformed regions in each one of these samples. The differences in interaction with the surface explains the splitting in the energy position of these Raman modes. As can be seen in Table I, the pressure evolution of the out-of-plane modes (${A_{1g}}^{(h)}$ (${A_1}^{(h)}$), ${A_{1g}}^{(\ell)}$ (${A_1}^{(h)}$)) and of the unbound ${E^1_{2g}}^{(\ell)}$ (${E'}^{(\ell)}$) mode are within error bars independent of the number of layers or at most a slightly decreasing function of n. On the other side the ${E^1_{2g}}^{(h)}$ (${E'}^{(h)}$) mode exhibits a very different pressure slope with respect to the ${E^1_{2g}}^{(\ell)}$ (${E'}^{(\ell)}$) mode as well as a strong dependence with n between the monolayer and the bilayer sample. We will come later to provide an explanation to this effect.

We note the absence in the trilayer sample as well as the many-layer one of any Raman component corresponding to regions highly conformed to the surface roughness. This can be easily understood from the evolution of the bending rigidity and adhesion with the number of layers. In fact, the bending rigidity D_n is an increasing function of n which varies as $D_n = D_1 n^3$ assuming that sliding between the layers is negligible. In the case of graphene, experiments [51] show an even faster evolution with n than the above referred power law: $D_{Graphene}(1) = 7.1^{+4.0}_{-3.0}$ eV, $D_{Graphene}(2) = 35.5^{+20.0}_{-15.0}$ eV and $D_{Graphene}(3) = 126^{+71.0}_{-53.0}$ eV. We should note that this D_1 value seems to be overestimated when compared with the different values compiled from literature [52]. The adhesion energy, γ_n, on its side should be a weakly varying function of n. We then expect that the ratio of surfaces low-conformed and high-

conformed, $S_\ell(n)/S_h(n)$ is a rapidly increasing function of n. Our experiments show that in MoS_2 lying on SiO_2 substrate with as grown roughness, $S_h(n) \to 0$ for $n > 2$.

The differences in the bending rigidity between the mono and the bilayer samples can also explain the observed differences between the high pressure behavior of their high conformation components. First we may consider the differences concerning the intensity of the signal. The rapid attenuation in the monolayer sample of the "(h)" components of the Raman signal can be interpreted as due to a rapid increase of $S_\ell(n)/S_h(n)$ related to the progressive penetration of the liquid pressure transmitting medium between the substrate and the monolayer sample. In bilayer MoS_2, the higher bending rigidity, implies a higher elastic energy needed to unbind the MoS_2 bilayer explaining why the highly conformed component is present until the higher pressures of our study. Such differences can also be related to the observed broadening of $A_1^{(h)}$ for the monolayer sample with respect to the bilayer one (Figure 2).

We should also consider factors affecting the MoS_2 $D(n)$ evolution with the number of layers by extending the analytical expression proposed in Ref. [53] for graphene. The result is that the value of $D(n)$ is only reduced by less than 10 % for $n = 2$ and $n = 3$ and we can then consider in first approximation such effect as negligible.

We may now turn to the observed variation of $\partial E_{2g}^{1\ (h)}/\partial P$ with n as shown in Table I. For high-pressure experiments is common to consider that a hydrostatic or quasi-hydrostatic pressure is transferred from the PTM to sample. However, for 2D systems supported on a substrate this assumption is not valid [54]. The substrate deformation by the effect of pressure is transmitted as a biaxial stress to the 2D sample if that layer is well conformed to the substrate. Consequently, a plot of Raman shift versus pressure is not appropriated, since the pressure derivative does not represent an intrinsic response of the 2D material, but it depends on the mechanical properties of the substrate. We need then to consider the biaxial stress transmitted from the SiO_2 substrate to the MoS_2 layers. The MoS_2 biaxial stress is linked to the applied pressure through[54]:

$$\sigma_{MoS_2} = \theta(n)\frac{\beta_{MoS_2}}{\beta_{SiO_2}}P, \tag{1}$$

where $\theta(n)$ is the strain transfer efficiency, that can vary from 1 (total strain transfer) to

0 (fully unbinding MoS_2 from the SiO_2). This parameter is dependent on the number of layers and on the substrate properties [54]. In our case the substrate is the same for all n values and we can then assume $\theta(n)$ as being only dependent on the number of layers. The parameters β_{MoS_2} and β_{SiO_2} are the linear in plane stiffness constants of MoS_2 and of the substrate, respectively, having values of $\beta_{MoS_2} = 190$ GPa [28] and $\beta_{SiO_2} = 114$ GPa [54]. This equation gives us a relation between the pressure slope of those Raman modes involving bond vibrations in the direction of the biaxial stress, i.e., in our case the $E^1_{2g}(n)$ mode, and the pressure coefficient of the corresponding Raman mode in the bulk:

$$\frac{\partial \omega_{E^1_{2g}}(n)}{\partial P} \approx \theta(n) \frac{\beta_{MoS_2}}{\beta_{SiO_2}} \frac{\partial \omega_{E^1_{2g}}(Bulk)}{\partial P} \tag{2}$$

where we have assumed as a zero order approximation that for high values of θ the in-plane Raman mode evolution is essentially governed by the biaxial strain effects. Considering the values in the literature for $\partial \omega_{E^1_{2g}}(Bulk)/\partial P$ ranging from 1.7 to 1.9 cm^{-1}/GPa^{-1} leads to a value of $\partial \omega_{E^1_{2g}}(Bulk)/\partial P$ =3.0±0.3 cm^{-1}/GPa^{-1} when taking $\theta(1)$ =1. This value is in excellent agreement with the experimental result in single layer highly conformed MoS_2, meaning that the fraction of the surface being highly conformed to the surface, $S_a(1)$ is also highly biaxially strained ($\theta(1) \sim 1$), explaining the higher pressure slope of the E'$^{(h)}$ mode. In addition when expressed as function of the strain we obtain $\partial \omega_{E'^{(h)}(1)}/\partial \epsilon = 3.8 \pm 0.4$ $cm^{-1}/\%$ in rather good agreement with published values [44].

In the case of $n = 2$ the fact that $\partial \omega_{E^1_{2g}{}^{(h)}(2)}/\partial P < \partial \omega_{E'^{(h)}(1)/\partial P}$ means that $\theta(2) < \theta(1)$ and should tend to zero for $n = 3$. The determination of the exact value of $\theta(n)$ for $n > 1$ needs a deeper understanding on the compression process and in particular on the simultaneous participation of hydrostatic and biaxial strain components on a system which contrarily to graphene involves out-of-plane chemical bonds. In Figure 4 are shown the different values for the E^1_{2g} and A_{1g} pressure slopes highlighting the transition from the bimodal adhesion behaviour for n=1,2 to single low conformation adhesion for $n > 2$.

To conclude, it is interesting to consider the reasons that make that the mechanical response of MoS_2 on SiO_2 at high pressure differs significantly from the one of graphene on SiO_2. We can underline two distinctive aspects:

1) MoS_2 shows for n=1,2 the presence of mixed high and low conformed regions and total

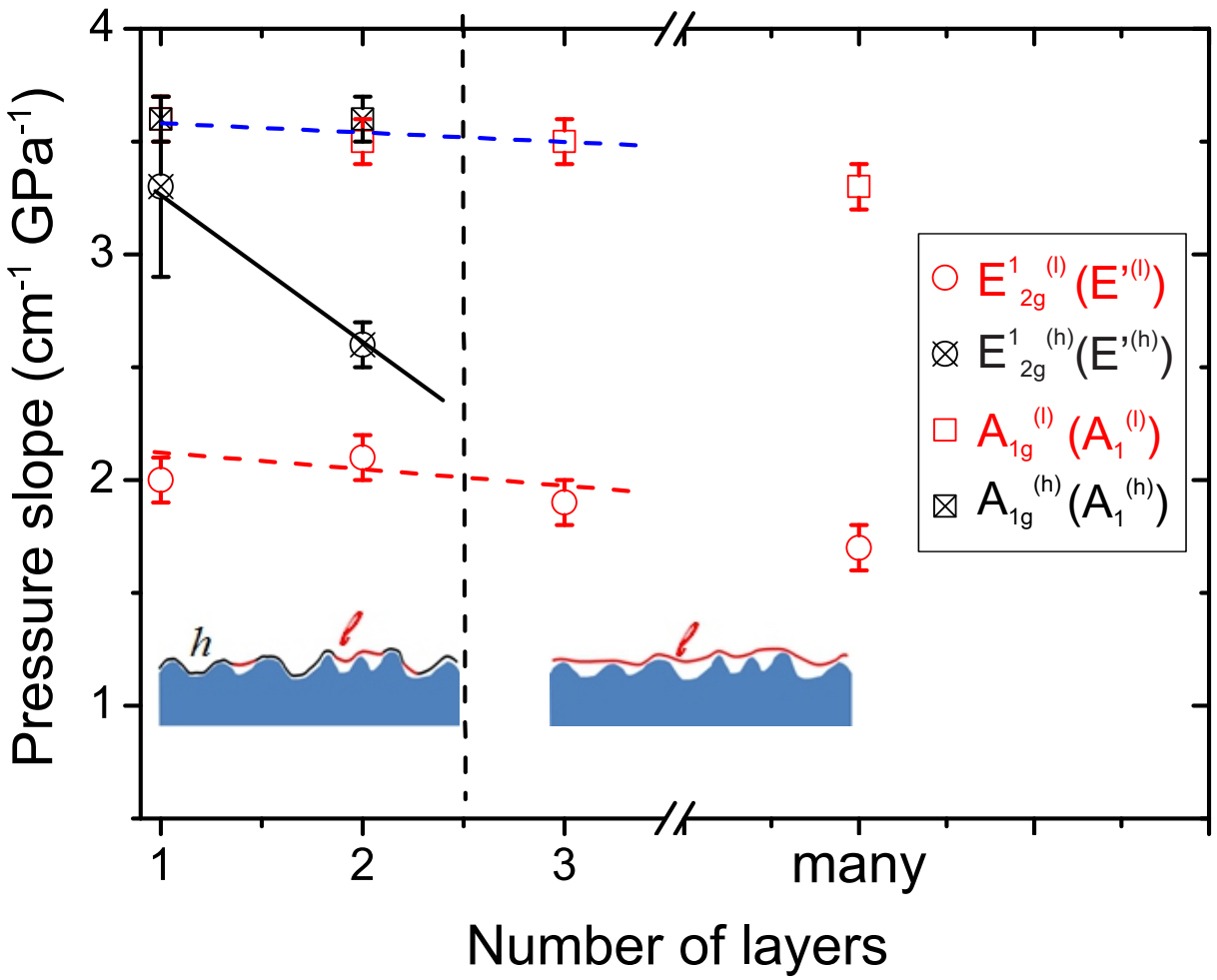

FIG. 4. Pressure slopes of the E^1_{2g} and A_{1g} modes as function of the number of MoS_2 layers. The two different high ((h), black) and low ((ℓ), red) conformation components are separated. The lines are guides for the eye. We have underlined the sensitivity of the $E^1_{2g}{}^{(h)}$ $E'^{(h)}$ component to the biaxial strain generated by substrate compression. The drawings at the bottom of the figure sketch the bimodal and single adhesion situations.

unbinding for $n > 2$. In graphene such bimodal behavior was not observed. Graphene shows strong adhesion for n=1,2 and total unbinding from a SiO_2 substrate for $n > 2$ [37]. Such differences are related to the higher bending modulus of MoS_2.

2) For single layer MoS_2 on SiO_2, the highly conformed regions have values of $\theta(1) \sim 1$ whereas for graphene on SiO_2, the biaxial strain transfer is much smaller with $\theta(1) \sim 0.2$ [54]. Such strong difference is explained from the strong differences on in-plane compressibility between MoS_2 and graphene with respect to the one of the SiO_2 substrate. Graphene being much less compressible is not able to follow the deformations imposed by the high biaxial strain provided by the SiO_2 substrate during its compression, whereas the highly conformed

MoS_2 regions, with an in-plane compressibility much closer to the one of silica, deforms at the same rate that the substrate.

CONCLUSIONS

We performed a high pressure non-resonant Raman study on mechanically exfoliated MoS_2 deposited on SiO_2. A splitting of the E^1_{2g} and A_{1g} modes were observed for the n=1 and 2 samples which is enhanced with increasing pressure. Such splitting, absent for $n > 2$, is interpreted as due to the simultaneous presence of regions high and low conformed to the substrate roughness respectively. Only the regions highly conformed to the surface show a significant evolution of the of the E^1_{2g} mode pressure slope with the number of layers. The absolute values of such slopes is explained in terms of the biaxial strain transfer from the substrate and its evolution with the number of layers as due to the evolution of the efficiency of transfer from the substrate. The differences of in plane compressibility between MoS_2 and the substrate and the evolution of the bending rigidity of MoS_2 with the number of layers are discussed as being the physical parameters governing the observed behavior.

Brazilian authors acknowledge funding from CNPq (grant 307317/2010-2, INCT NanoBioSimes) and Central Analítica-UFC/CT-INFRA-FINEP/Pró-Equipamentos-CAPES/CNPq-SisNano-MCTI (grant 402284/2013-5). R. S. Alencar is also in debt to Coordenação de Aperfeiçoamento de Pessoal de Nível Superior (CAPES) under the grant No. 99999.004227/2014-00 for financial support.

[1] K. S. Novoselov, A. K. Geim, S. V. Morozov, D. Jiang, Y. Zhang, S. V. Dubonos, I. V. Grigorieva, and A. A. Firsov, Science **306**, 666 (2004), http://www.sciencemag.org/content/306/5696/666.full.pdf.

[2] Y. Zhu, S. Murali, W. Cai, X. Li, J. W. Suk, J. R. Potts, and R. S. Ruoff, Advanced Materials **22**, 3906 (2010).

[3] X. Li and H. Zhu, Journal of Materiomics **1**, 33 (2015).

[4] Kumar, A. and Ahluwalia, P.K., The European Physical Journal B **85**, 186 (2012).

[5] Y.-H. Lee, L. Yu, H. Wang, W. Fang, X. Ling, Y. Shi, C.-T. Lin, J.-K. Huang, M.-T. Chang, C.-S. Chang, M. Dresselhaus, T. Palacios, L.-J. Li, and J. Kong, Nano Letters **13**, 1852

(2013), http://dx.doi.org/10.1021/nl400687n.

[6] A. L. Elías, N. Perea-López, A. Castro-Beltrán, A. Berkdemir, R. Lv, S. Feng, A. D. Long, T. Hayashi, Y. A. Kim, M. Endo, H. R. Gutiérrez, N. R. Pradhan, L. Balicas, T. E. Mallouk, F. López-Urías, H. Terrones, and M. Terrones, ACS Nano **7**, 5235 (2013), http://dx.doi.org/10.1021/nn400971k.

[7] S. V. Bhatt, M. P. Deshpande, V. Sathe, R. Rao, and S. H. Chaki, Journal of Raman Spectroscopy **45**, 971 (2014).

[8] H. Li, J. Wu, Z. Yin, and H. Zhang, Accounts of Chemical Research **47**, 1067 (2014), http://dx.doi.org/10.1021/ar4002312.

[9] J.-K. Huang, J. Pu, C.-L. Hsu, M.-H. Chiu, Z.-Y. Juang, Y.-H. Chang, W.-H. Chang, Y. Iwasa, T. Takenobu, and L.-J. Li, ACS Nano **8**, 923 (2014), http://dx.doi.org/10.1021/nn405719x.

[10] L. Zhou, K. Xu, A. Zubair, A. D. Liao, W. Fang, F. Ouyang, Y.-H. Lee, K. Ueno, R. Saito, T. Palacios, J. Kong, and M. S. Dresselhaus, Journal of the American Chemical Society **137**, 11892 (2015), http://dx.doi.org/10.1021/jacs.5b07452.

[11] R. B., R. A., B. J., G. V., and K. A., Nature Nanotechnology **6**, 147150 (2011).

[12] A. Castellanos-Gomez, M. Poot, G. A. Steele, H. S. J. van der Zant, N. Agraït, and G. Rubio-Bollinger, Advanced Materials **24**, 772 (2012).

[13] X. Dou, K. Ding, D. Jiang, and B. Sun, ACS Nano **8**, 7458 (2014), http://dx.doi.org/10.1021/nn502717d.

[14] B. Radisavljevic, M. B. Whitwick, and A. Kis, ACS Nano **5**, 9934 (2011), http://dx.doi.org/10.1021/nn203715c.

[15] E. Gourmelon, O. Lignier, H. Hadouda, G. Couturier, J. Bernde, J. Tedd, J. Pouzet, and J. Salardenne, Solar Energy Materials and Solar Cells **46**, 115 (1997).

[16] W. Ho, J. C. Yu, J. Lin, J. Yu, , and P. Li, Langmuir **20**, 5865 (2004), http://dx.doi.org/10.1021/la049838g.

[17] A. Splendiani, L. Sun, Y. Zhang, T. Li, J. Kim, C.-Y. Chim, G. Galli, and F. Wang, Nano Letters **10**, 1271 (2010), http://dx.doi.org/10.1021/nl903868w.

[18] K. F. Mak, C. Lee, J. Hone, J. Shan, and T. F. Heinz, Physical Review Letters **105**, 136805 (2010).

[19] H. Zeng and X. Cui, Chemical Society Reviews **44**, 2629 (2015).

[20] B. Chakraborty, H. S. S. R. Matte, A. K. Sood, and C. N. R. Rao, Journal of Raman Spectroscopy **44**, 92 (2013).

[21] A. Molina-Sánchez and L. Wirtz, Physical Review B **84**, 155413 (2011).

[22] K. F. Mak, K. He, J. Shan, and T. F. Heinz, Nature Nanotechnology **7**, 494498 (2012).

[23] A. San-Miguel, Chemical Society Reviews **35**, 876 (2006).

[24] C. Lee, H. Yan, L. E. Brus, T. F. Heinz, J. Hone, and S. Ryu, ACS Nano **4**, 2695 (2010), http://dx.doi.org/10.1021/nn1003937.

[25] K. Golasa, M. Grzeszczyk, R. Bożek, P. Leszczński, A. Wysmolek, M. Potemski, and A. Babiński, Solid State Communications **197**, 53 (2014).

[26] H. Li, Q. Zhang, C. C. R. Yap, B. K. Tay, T. H. T. Edwin, A. Olivier, and D. Baillargeat, Advanced Functional Materials **22**, 1385 (2012).

[27] Z.-H. Chi, X.-M. Zhao, H. Zhang, A. F. Goncharov, S. S. Lobanov, T. Kagayama, M. Sakata, and X.-J. Chen, Physical Review Letters **113**, 036802 (2014).

[28] N. Bandaru, R. S. Kumar, D. Sneed, O. Tschauner, J. Baker, D. Antonio, S.-N. Luo, T. Hartmann, Y. Zhao, and R. Venkat, The Journal of Physical Chemistry C **118**, 3230 (2014), http://dx.doi.org/10.1021/jp410167k.

[29] F. Li, Y. Yan, B. Han, L. Li, X. Huang, M. Yao, Y. Gong, X. Jin, B. Liu, C. Zhu, Q. Zhou, and T. Cui, Nanoscale **7**, 9075 (2015).

[30] X. Fan, C.-H. Chang, W. T. Zheng, J.-L. Kuo, and D. J. Singh, The Journal of Physical Chemistry C **119**, 10189 (2015), http://dx.doi.org/10.1021/acs.jpcc.5b00317.

[31] H. Guo, T. Yang, P. Tao, Y. Wang, and Z. Zhang, Journal of Applied Physics **113**, 013709 (2013).

[32] L. Hromadová, R. Martoňák, and E. Tosatti, Physical Review B **87**, 144105 (2013).

[33] A. P. Nayak, S. Bhattacharyya, J. Zhu, J. Liu, X. Wu, Tribhuwan, Pandey, C. Jin, A. K. Singh, D. Akinwande, and J.-F. Lin, Nature Communications **5** (2014), 10.1038/ncomms4731.

[34] T. Livneh and E. Sterer, Physical Review B **81**, 195209 (2010).

[35] A. P. Nayak, T. Pandey, D. Voiry, J. Liu, S. T. Moran, A. Sharma, C. Tan, C.-H. Chen, L.-J. Li, M. Chhowalla, J.-F. Lin, A. K. Singh, and D. Akinwande, Nano Letters **15**, 346 (2015), http://dx.doi.org/10.1021/nl5036397.

[36] J. Shang, L. Zhang, X. Cheng, and F. Zhai, Solid State Communications **219**, 33 (2015).

[37] J. Nicolle, D. Machon, P. Poncharal, O. Pierre-Louis, and A. San-Miguel, Nano Letters **11**, 3564 (2011), http://dx.doi.org/10.1021/nl201243c.

[38] K. S. Novoselov and A. H. C. Neto, Physica Scripta **2012**, 014006 (2012).

[39] N. A. Lanzillo, A. Glen Birdwell, M. Amani, F. J. Crowne, P. B. Shah, S. Najmaei, Z. Liu, P. M. Ajayan, J. Lou, M. Dubey, S. K. Nayak, and T. P. O'Regan, Applied Physics Letters **103**, 093102 (2013).

[40] S. Klotz, J.-C. Chervin, P. Munsch, and G. L. Marchand, Journal of Physics D: Applied Physics **42**, 075413 (2009).

[41] H. Mao, J. Xu, and P. Bell, Journal of Geophysical Research **91**, 4673 (1986).

[42] A. Bagnall, W. Liang, E. Marseglia, and B. Welber, Physica B+C **99**, 343 (1980).

[43] S. Sugai and T. Ueda, Phys. Rev. B **26**, 6554 (1982).

[44] H. J. Conley, B. Wang, J. I. Ziegler, J. Richard F. Haglund, S. T. Pantelides, and K. I. Bolotin, Nano Letters **13**, 3626 (2013), http://dx.doi.org/10.1021/nl4014748.

[45] C. R. Zhu, G. Wang, B. L. Liu, X. Marie, X. F. Qiao, X. Zhang, X. X. Wu, H. Fan, P. H. Tan, T. Amand, and B. Urbaszek, Physical Review B **88**, 121301 (2013).

[46] O. Pierre-Louis, Physical Review E **78**, 021603 (2008).

[47] J.-W. Jiang, Z. Qi, H. S. Park, and T. Rabczuk, Nanotechnology **24**, 435705 (2013).

[48] P. Li, Z. You, and T. Cui, J. Micromech. Microeng. **23**, 045026 (2013).

[49] J. Quereda, A. Castellanos-Gomez, N. Agrat, and G. Rubio-Bollinger, Applied Physics Letters **105**, 053111 (2014).

[50] W. G. Cullen, M. Yamamoto, K. M. Burson, J. H. Chen, C. Jang, L. Li, M. S. Fuhrer, and E. D. Williams, Phys. Rev. Lett. **105**, 215504 (2010).

[51] N. Lindahl, D. Midtvedt, J. Svensson, O. A. Nerushev, N. Lindvall, A. Isacsson, and E. E. B. Campbell, Nano Letters **12**, 3526 (2012), http://dx.doi.org/10.1021/nl301080v.

[52] P. Lambin, Applied Sciences **4**, 282 (2014).

[53] P. Koskinen and O. O. Kit, Physical Review B **82**, 235420 (2010).

[54] C. Bousige, F. Balima, D. Machon, G. S. Pinheiro, A. Torres-Dias, J. Nicolle, D. Kalita, N. Bendiab, L. Marty, V. Bouchiat, G. Montagnac, A. G. Souza Filho, P. Poncharal, and A. San-Miguel, Nano Letters **17**, 21 (2017), http://dx.doi.org/10.1021/acs.nanolett.6b02981.